



Contents lists available at ScienceDirect

Journal of King Saud University – Science

journal homepage: www.sciencedirect.com



Original article

Green synthesis of gold nanoparticles using *Jatropha integerrima* Jacq. flower extract and their antibacterial activity

Gunasekaran Suriyakala^a, Sivaji Sathiyaraj^a, Ranganathan Babujanarthanam^{a,*}, Khaloud Mohammed Alarjani^b, Dina S. Hussein^c, Rabab Ahmed Rasheed^d, K. Kanimozhi^e^a Nano and Energy Bioscience Laboratory, Department of Biotechnology, Thiruvalluvar University, Serkkadu, Vellore 632115, Tamil Nadu, India^b Department of Botany and Microbiology, College of Science, King Saud University, Riyadh 11451, Saudi Arabia^c Department of Chemistry, College of Sciences and Health, Cleveland State University, Cleveland 44115, United States^d Histology & Cell Biology Department, Faculty of Medicine, King Salman International University, South Sinai, Egypt^e Department of Chemistry, Global Institute of Engineering and Technology (GIET), Melvisharam 632509, Tamil Nadu, India

ARTICLE INFO

Article history:

Received 17 November 2021

Revised 12 December 2021

Accepted 9 January 2022

Available online 17 January 2022

Keywords:

Gold nanoparticles

Jatropha integerrima Jacq.

TEM

Antibacterial activity

Escherichia coli

ABSTRACT

Background: With the rise of antibiotic resistance, there is an increasing interest in discovering novel antimicrobial agents. Antibiotics could be replaced with metal-based nanoparticles that have long-lasting antibacterial properties. This study aimed to synthesize gold nanoparticles (AuNPs) and test their antibacterial effectiveness against a variety of human pathogens.

Methods: The AuNPs were characterized using UV, FT-IR, XRD, and TEM with EDX. By using the well diffusion and microdilution techniques, the impact of synthesized AuNPs was tested against *B. subtilis*, *S. aureus*, *E. coli*, and *K. pneumoniae*.

Results: The AuNPs were synthesized from *Jatropha integerrima* Jacq. flower extract. UV-vis spectrum showed a high peak at 547 nm; FT-IR revealed phenolic compounds in the plant extract were responsible for AuNP formation. XRD and SAED confirmed the crystalline nature while TEM revealed the shape to be spherical and DLS revealed the size to be 38.8 nm with the stability of -0.3 mV. The AuNPs exhibit maximal and minimal antibacterial activity towards *E. coli* and *B. subtilis*. The MIC of AuNPs against *B. subtilis*, *S. aureus*, *E. coli*, and *K. pneumoniae* were found to be 5.0, 10, 2.5, and 2.5 $\mu\text{g/mL}$, respectively.

Conclusion: Thus, synthesized nanoparticles might be a good alternative to develop an antibacterial agent against the selected human pathogens.

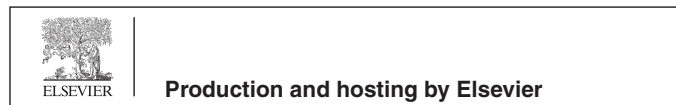
© 2022 The Author(s). Published by Elsevier B.V. on behalf of King Saud University. This is an open access article under the CC BY-NC-ND license (<http://creativecommons.org/licenses/by-nc-nd/4.0/>).

Abbreviations: ATCC, American Type Culture Collection; AuNPs, Gold nanoparticles; DLS, Dynamic Light Scattering; EDX, Energy dispersive X-ray analysis; FTIR, Fourier Transform Infra-Red Spectroscopy; JIF-AuNPs, Synthesized gold nanoparticles; MIC, Minimum inhibitory concentration; MTCC, Microbial Type Culture Collection; PDI, Polydispersity index; SAED, Selected area diffraction pattern; SPR, Surface plasmon resonance; TEM, Transmission Electron Microscopy; UV-Vis, UV-Visible spectroscopy; XRD, X-ray Diffraction spectroscopy; ZOI, Zone of inhibition.

* Corresponding author.

E-mail address: babukmg@gmail.com (R. Babujanarthanam).

Peer review under responsibility of King Saud University.



<https://doi.org/10.1016/j.jksus.2022.101830>

1018-3647/© 2022 The Author(s). Published by Elsevier B.V. on behalf of King Saud University.

This is an open access article under the CC BY-NC-ND license (<http://creativecommons.org/licenses/by-nc-nd/4.0/>).

1. Introduction

Disease-causing microbes have become drug-resistant through the adequate usage of antibiotics (Maiti et al., 2014). Different forms of bacteria are developing resistance to currently available antibiotics, posing a severe threat to public health. Antibiotics are ineffective in treating illnesses caused by drug-resistant bacteria. Such antibiotic resistance needs a stronger alternative solution (Adil et al., 2019). In this situation, there is a higher need for novel bactericides to be developed to avoid a threat to public health.

As a result, it is critical to create effective and low-cost techniques for the synthesis of therapeutic agents to combat the aforementioned health issues. Nanotechnology is expanding possibilities, enabling new solutions to be developed using existing resources. Metals, semiconductors, and metal oxides are employed in nanotechnology for a broad range of applications in information, energy, environmental, and medicinal sectors (Heera and

Shanmugam, 2015). Gold nanoparticles (AuNPs) have sparked interest among existing nanomaterials because gold is an inert, oxidation-resistant substance, which makes its use interesting in nanoscale technologies and devices (Bindhu and Umadevi, 2014). Because of their numerous applications, such as drug transport, chemical, and biological imaging, catalysis, therapeutics, and diagnostics, AuNPs are the most intensively investigated NPs of all metals (Sathiyaraj et al., 2021). Furthermore, the reduction and functionalization of AuNPs with synthetic and natural compounds are well understood. Physical and chemical methods are commonly used to make AuNPs, which are both expensive and dangerous to the environment. As a result, the biosynthesis of nanoparticles has recently gotten a lot of attention because the nanoparticles produced are non-toxic and can be employed in biomedical applications (Priya Velammal et al., 2016). Plants, plant wastes, plant components, bacteria, and fungi have all been employed to synthesize nanoparticles in the past several years (Otunola et al., 2017). Plants are superior possibilities for nanoparticle production since they are generally nontoxic, provide natural capping agents, and minimize the expense of microbe isolation and culture media (Krithiga et al., 2015).

There are no reports on the use of *Jatropha integerrima* Jacq. for the synthesis of AuNPs. Thus, the current research, it was aimed to investigate the formation of AuNPs from flower extract of *Jatropha integerrima* Jacq. and the synthesized AuNPs (JIF-AuNPs) were confirmed by UV-Visible spectroscopy (UV-Vis), Fourier Transform Infra-Red Spectroscopy (FTIR), Transmission Electron Microscopy (TEM), Selected area diffraction pattern (SAED), Energy dispersive X-ray analysis (EDX), particle and zeta potential analysis and X-Ray Diffraction spectroscopy (XRD). The antibacterial and minimum inhibitory concentration (MIC) effect of the JIF-AuNPs were investigated against pathogenic bacteria including, *B. subtilis* (MTCC 2394), *S. aureus* (ATCC 25923), *E. coli* (MTCC 448), and *K. pneumoniae* (MTCC 109).

2. Materials and methods

2.1. Plant collection and authentication

The flower sample was collected from the Thiruvalluvar University campus at Vellore, Tamil Nadu, India. Dr. Jayaraman verified and authenticated the collected flowers as *Jatropha integerrima* Jacq. (PARC/2019/4026), and the voucher was deposited at the Herbarium of the Plant Anatomy Research Centre in Tambaram, Chennai, Tamil Nadu, India.

2.2. Preparation of flower sample

To eliminate dust particles, the flower material was cleaned with deionized water and air-dried to remove moisture content. The flower sample was then weighed and homogenized before being transferred to a 250 mL screw cap container containing 100 mL distilled water. The container was placed in a magnetic stirrer for 10–15 min to ensure adequate mixing, after which the aqueous extract was filtered and kept at 4 °C in an airtight container.

2.3. Synthesis of AuNPs

For the synthesis of AuNPs, 10 mL of aqueous extract was mixed with 90 mL of 1 mM AuCl₃ solution and the color shift was noticed. The AuNPs solution was then spun at 10,000 rpm for 15 min at 4 °C to purify it. The resulting pellet was then dried and stored at room temperature for future use after being suspended in deionized water.

2.4. Characterization of JIF-AuNPs

2.4.1. UV-Vis analysis

To test the bio-reduction property, the Shimadzu UV-1800 spectrometer was employed to record the UV-Vis spectrum of gold suspension. For spectrum analysis, 3 mL of the reaction mixture was placed in a quartz cuvette. Spectral analysis was performed on wavelengths ranging from 300 nm to 700 nm (Mani et al., 2021c).

2.4.2. FTIR

FTIR was used to evaluate the functional groups contained in the biosynthesized JIF-AuNP. The mixture of 2.5 mg dried JIF-AuNP powder and 250 mg potassium bromide was placed in an FTIR sample container. The mixture was then analyzed using a Shimadzu FTIR-8400S at a range of 500–4000 cm⁻¹ spectra (Gandhi et al., 2021).

2.4.3. TEM

The HITACHI h-800 was used to discover the shape, and size of nanoparticles through TEM analysis. Samples were suspended in double-distilled water for the TEM-grid preparation, and then a single drop of the suspended sample was added on a copper grid covered with carbon and dried under a light. Image J software was used to measure the size of AuNPs.

2.4.4. EDX analysis

The existence of gold in the produced gold nanoparticles was confirmed by EDX analysis. A microscopic slide was drop-coated with gold nanoparticles and dried at 50 °C using a hot air oven. The slide was analyzed and the signals were recorded using an EDX microscopic analysis system combined with TEM.

2.4.5. SAED pattern analysis

The SAED pattern was used to examine the structural crystallinity of synthesized JIF-AuNP. To avoid contaminant interactions, the sample was prepared with millipore filtered water and then analyzed.

2.4.6. Particle size analysis

The JIF-AuNPs liquid suspension was drained through a syringe filter, and the nanoparticle size was calculated using a particle size analyzer.

2.4.7. Zeta potential measurement

The electrical potential in the double layer of ions encircling a particle at the particle surface's boundary and the adsorbed ions in the diffuse layer are characterized by the zeta potential (Koperuncholan, 2015).

2.4.8. XRD

XRD analysis of the JIF-AuNPs was done using Bruker D8-Advance XRD analyzer, at a process voltage of 40 kV and a current of 30 mA with Cu K α radiation (Rathnakumar et al., 2019). The XRD peaks were captured at 2 θ at a scanning speed of 0.02°/min from 20° to 80° (George et al., 2020). The following Debye-Scherrer formula was used to compute the average particle size (Mani et al., 2021b).

$$D = \frac{k\lambda}{\beta \cos\theta}$$

where D = particle size, k = Scherrer constant (value = 0.9), λ = wave length of the x-ray sources (0.15406 nm), β = full width at half maximum, and θ = peak position.

2.5. Antibacterial activity

The inhibitory effect of JIF-AuNPs *B. subtilis*, *S. aureus*, *E. coli*, and *K. pneumoniae* was determined by the agar well diffusion method (Suriyakala et al., 2021). The freshly grown selected organisms were sub-cultured on petri plates containing a sterilized Mueller-Hinton (MH) agar medium. The 8 mm wells were made with a sterile cork borer and then varied concentrations (10, 20, 30, 40 $\mu\text{g/mL}$) of JIF-AuNPs were loaded in the well. Then, the agar plates were kept in an incubator at an optimum temperature for a day. After incubation, a clear zone around the wells was observed and measured. The results were compared with 10 $\mu\text{g/mL}$ of standard control (Ampicillin).

2.6. MIC

The MIC was calculated using repeated two-fold dilutions of JIF-AuNPs in various concentrations ranging from 2.5 to 10 $\mu\text{g/mL}$ in MH broth. The MH broth containing the selected isolates and various quantities of JIF-AuNPs served as the positive control, whereas the negative control contained only the selected isolates. The MIC is the lowest concentration of JIF-AuNPs that suppresses bacterial growth by 99%. The visible turbidity of the tubes before and after incubation was used to evaluate the MIC of the selected isolates (Parvekar et al., 2020).

3. Results

3.1. Synthesis and optical characterization of JIF-AuNPs

The formation of nanoparticles was preliminarily identified by the color change from pale pink to ruby red (Fig. 1), which suggested the synthesis of AuNPs. A sharp single absorption peak was observed at 547 nm, which corresponds to the surface plasmon resonance (SPR) band of JIF-AuNPs (Veena et al., 2019) (Fig. 2). The energy band gap was analyzed by the Tauc plot method using UV data and it was found to be 1.9 eV (Fig. 3). For analyzing the functional groups present in a nanoparticle, FTIR is a highly useful instrument. The FTIR spectra (Fig. 4) in our investigation ranged from 500 to 4000 cm^{-1} . Fig. 3 shows the bands observed on the FTIR spectra of JIF-AuNPs at 3237, 2920, 1613, 1317, 1023, and 760 cm^{-1} .

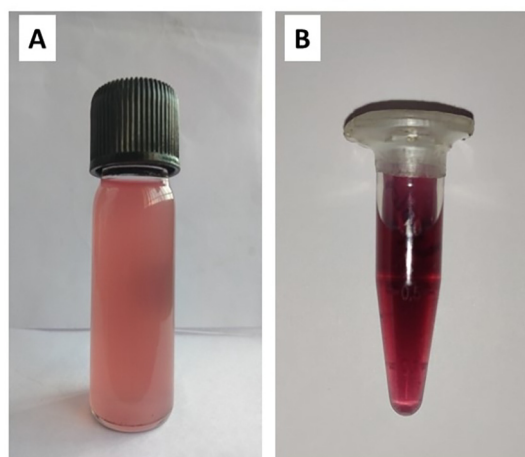


Fig. 1. Visual observation of nanoparticle formation. A) *Jatropa integerrima* Jacq. flower extract. B) Synthesized gold nanoparticles.

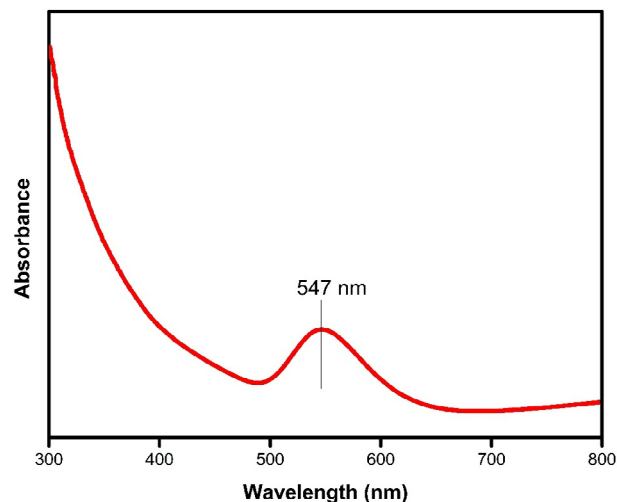


Fig. 2. UV-Vis spectrum of *Jatropa integerrima* Jacq. synthesized gold nanoparticles.

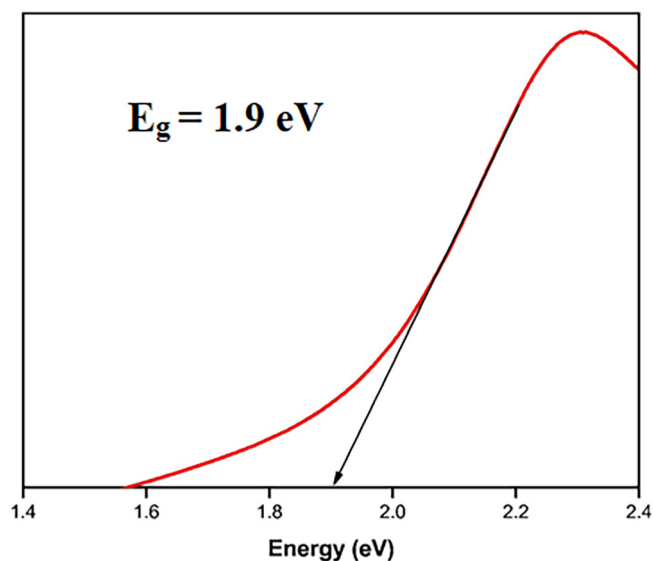


Fig. 3. Energy band gap analysis of JIF-AgNPs.

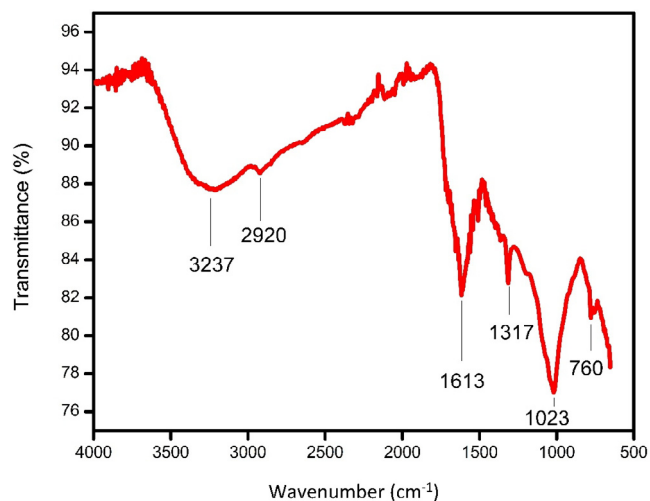


Fig. 4. Fourier transform infrared spectrum of JIF-AuNPs.

3.2. Morphological characterization of JIF-AuNPs

As shown in Fig. 5A, spherical-shaped nanoparticles with a size of 28 to 43 nm were obtained and an average size of the particles was discovered to be 37.7 nm using TEM analysis. (Fig. 5H). The elemental composition was studied by EDX analysis. The absorption of metallic gold nanocrystallites was characterized by strong EDX signals at 1.8, 2.1, and 2.5 keV. The polycrystalline nature of the JIF-AuNPs was depicted by the SAED pattern of the corresponding area observed under TEM. The well-resolved diffraction rings of polycrystalline gold may be seen in the diffraction pattern. A series of significant planes with hkl values (111, 200, 220, and 311) of JIF-AuNPs were represented by strong and moderate-intensity rings (Fig. 5I). The average size of the JIF-AuNPs was calculated as 38.8 nm, with a PDI of 1.52 (Fig. 6A) by dynamic light scattering analysis, and the zeta potential was discovered to be -0.3 mV (Fig. 6B). XRD analysis showed four strong diffraction peaks at 37.9° , 44.1° , 64.5° , and 77.5° which were correlated to the (111), (200), (220), and (311) planes respectively, and they were associated with the face-centered cubic structure of gold (ICDD No. 4-0783) (Fig. 7). The average size of the JIF-AuNPs was computed using the Scherrer formula and found to be 6.9 nm.

3.3. Antibacterial activity

The agar well diffusion method was used to test the antibacterial activity of the JIF-AuNPs against *B. subtilis*, *S. aureus*, *E. coli*, and *K. pneumoniae*. In terms of zone of inhibition (ZOI), JIF-AuNPs showed antibacterial efficacy against all of the species tested (Fig. 8). The maximal and minimal inhibitory zone against *E. coli* and *B. subtilis* were found to be 17.67 ± 0.21 and 10.56 ± 0.21 mm, respectively (Table 1). The MIC of JIF-AuNPs was evaluated by the broth dilution method. After the incubation period, the growth of the *B. subtilis*, *S. aureus*, *E. coli*, and *K. pneumoniae* was visibly suppressed by treated with 5, 10, 2.5, and 2.5 $\mu\text{g/mL}$ of JIF-AuNPs, and the absorbance measured at 600 nm was found to be 0.13, 0.24, 0.05, and 0.07, respectively (Table 2).

4. Discussion

4.1. Characterization of JIF-AuNPs

Jatropha integerrima Jacq. was utilized as a reducing and stabilizing agent in this experiment, and AuCl_3 (1 mM) was used as

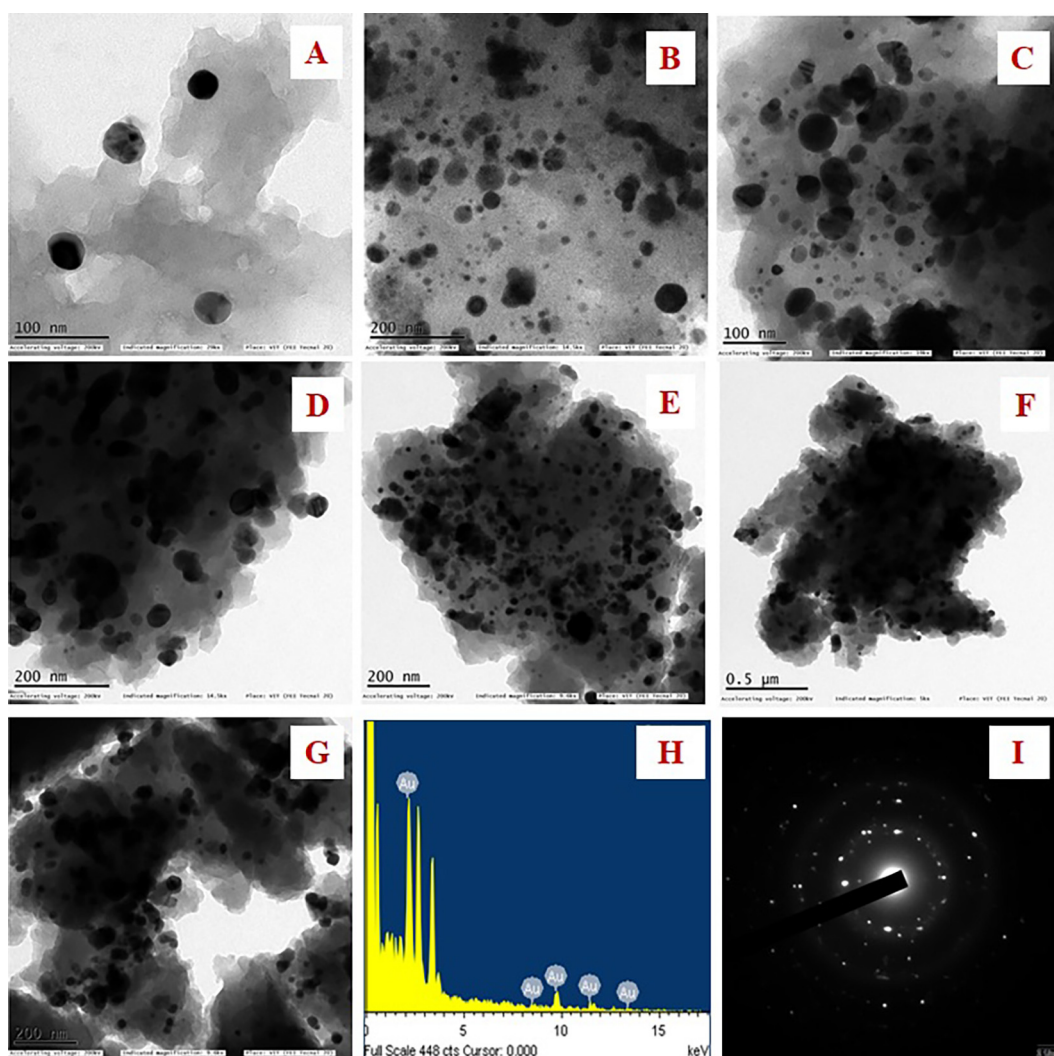


Fig. 5. A–G) TEM images of JIF-AuNPs at different nanometres. H) Elemental analysis of JIF-AuNPs. I) SAED pattern of JIF-AuNPs.

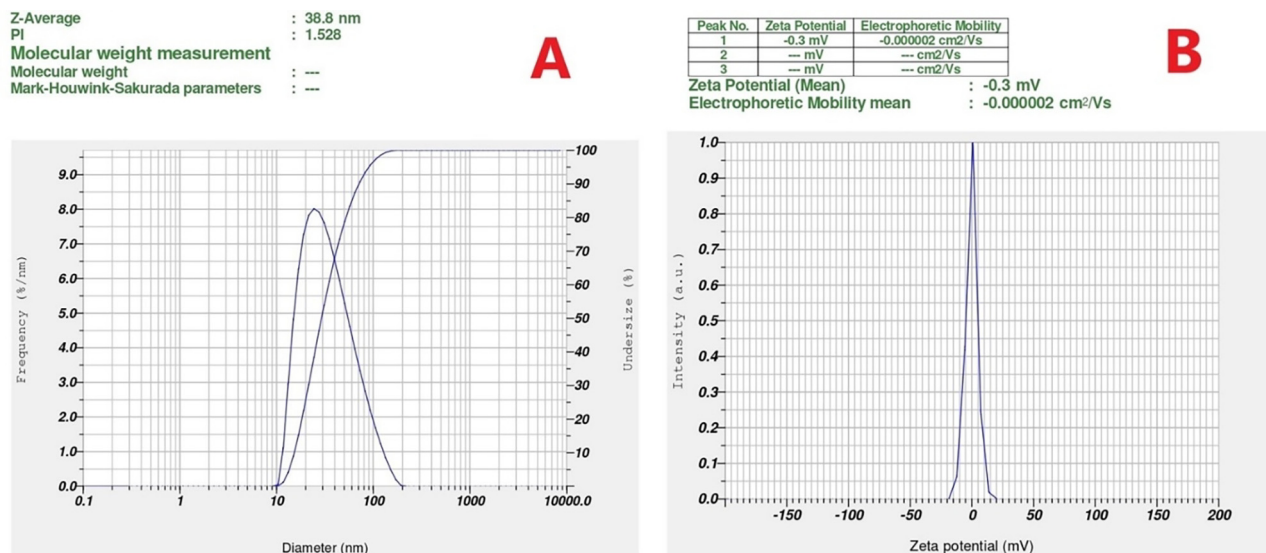


Fig. 6. DLS Measurements of JIF-AuNPs. A) Particle size, B) Zeta potential of JIF-AuNPs.

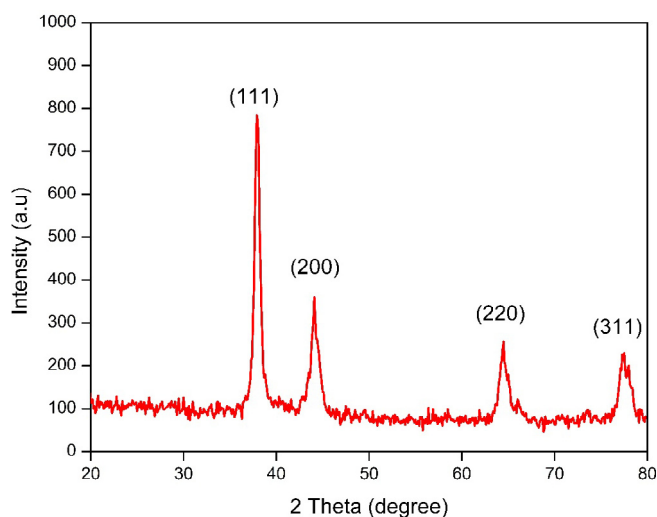


Fig. 7. X-ray diffraction peaks of JIF-AuNPs.

the gold precursor. For the formation of AuNPs, AuCl₃ was separated into Au⁺ and Cl₃⁻ ions in the aqueous solution of a reducing agent. As a consequence, Au⁺ ions are bound and capped by phytochemicals to form stable gold nanoparticles. The formation of AuNPs has been observed by examining the color change of the reaction mixture, as reported in the literature (Mittal et al., 2013). Noble metals exhibit SPR at the nanoscale, which accounts for the color change (Veena et al., 2019). The SPR is a remarkable phenomenon that occurs in metal nanoparticles which results in high electromagnetic fields on the particle surface, increasing all radiative characteristics like scattering and absorption. The optical characteristics of metal nanoparticles are widely known to be substantially influenced by their size and form. Due to the extra-fine nature and small size of the gold nanoparticles, previous findings revealed that the spherical gold nanoparticles offer absorption bands at roughly 525–555 nm in the UV–visible spectra (Saqr et al., 2021). The absorbance of gold nanoparticles was found to be approximately 547 nm in many investigations (Balasubramanian et al., 2020; Nadaroglu et al., 2017). The energy band gap was done by the method Tauc plot (Ramesh et al., 2019) and it was found to

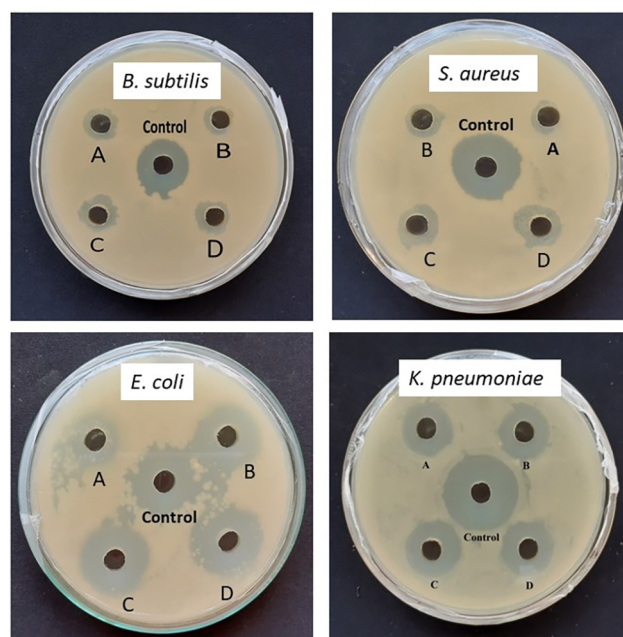


Fig. 8. Antibacterial activity of JIF-AuNPs at different concentration (A – 10 µg/mL, B – 20 µg/mL, C – 30 µg/mL, D – 40 µg/mL, and Control – 10 µg/mL of ampicillin).

be 1.9 eV. The low energy band gap reveals that the JIFF-ANPs effectively absorb the UV light (Raja et al., 2019).

The FTIR spectrum showed various peaks. The broad peaks seen at 3237 cm⁻¹ correspond to the phenolic –OH group found in the flower extract (Sk et al., 2020). The absorption band at 2920 cm⁻¹ belonged to the C–H stretching of the aliphatic or methylene group (Nithiyavathi et al., 2021). The free amine groups or carboxylate ion of the amino acid residues were identified at 1613 cm⁻¹. The band at 1317 cm⁻¹ shows C–N stretching, which is prevalent in proteins, demonstrating that protein acts as a ligand for AuNPs, increasing the stability of produced nanoparticles (Mittal et al., 2013). The OH stretching of the phenol group was visible in the band at 1023 cm⁻¹ (Raj Meena et al., 2020). The C–H stretching of aromatic compounds correlates to the band at

Table 1

ZOI of different bacterial species using JIF-AuNPs. The results were expressed as mean \pm standard error. Different superscript represents the results were significantly differ from each other according to Duncan's method ($p < 0.05$).

Strain	ZOI (mm)				
	10 $\mu\text{g/mL}$	20 $\mu\text{g/mL}$	30 $\mu\text{g/mL}$	40 $\mu\text{g/mL}$	Control 10 $\mu\text{g/mL}$
<i>B. subtilis</i>	8.33 \pm 0.14 ^e	8.67 \pm 0.21 ^d	9.42 \pm 0.18 ^c	10.56 \pm 0.21 ^b	14.33 \pm 0.13 ^a
<i>S. aureus</i>	8.56 \pm 0.27 ^e	9.0 \pm 0.08 ^d	10.47 \pm 0.24 ^c	11.33 \pm 0.23 ^b	16.33 \pm 0.15 ^a
<i>E. coli</i>	12.67 \pm 0.14 ^e	13.67 \pm 0.12 ^d	15.33 \pm 0.13 ^c	17.67 \pm 0.21 ^b	16.52 \pm 0.08 ^a
<i>K. pneumoniae</i>	13.42 \pm 0.14 ^e	14.53 \pm 0.18 ^d	15.42 \pm 0.18 ^c	15.67 \pm 0.24 ^b	21.33 \pm 0.12 ^a

Table 2

MIC value of selected human pathogenic bacteria using JIF-AuNPs.

S. No	Organism	MIC ($\mu\text{g/mL}$)	Absorbance at 600 nm
1	<i>B. subtilis</i>	5	0.13
2	<i>S. aureus</i>	10	0.24
3	<i>E. coli</i>	2.5	0.05
4	<i>K. Pneumoniae</i>	2.5	0.07

760 cm^{-1} , which is the typical vibration of the phenol group (Ibarra-Sánchez et al., 2015; Susan et al., 2017). The phenolic groups that aid in the synthesis of JIF-AuNPs are represented by the majority of the peaks. The size, structure, and particle distribution of JIF-AuNPs were studied using a TEM analysis (Folorunso et al., 2019). Spherical-shaped nanoparticles with an average size of 37.7 nm were found using TEM analysis. The elemental composition in the JIF-AuNPs was confirmed using EDX analysis (Theophil Anand et al., 2019). EDX spectrum showed strong signals at 1.8, 2.1, and 2.5 keV. Dhanasekar et al. (2015) discovered similar gold signals. The presence of randomly oriented particles with diameters in the nanometer range and their crystallinity were confirmed by SAED patterns in the form of diffraction rings. The diffraction rings observed indicated the crystalline nature of the JIF-AuNPs (Devanesan et al., 2021).

The hydrodynamic particle size, polydispersity index (PDI), and zeta potential of JIF-AuNPs were studied by DLS analysis (Mani et al., 2021a). The particle size was similar to the size estimated from the TEM image. JIF-AuNPs have a negative zeta potential, indicating that the stability of the JIF-AuNPs was due to the presence of negatively charged functional groups from the flower extract (Hemlata et al., 2020; Mariadoss et al., 2019). To obtain crystallographic information of metallic nanoparticles, X-ray diffraction analysis is commonly used. The JIF-AuNPs had a crystalline structure, as evidenced by the characteristic diffraction patterns in terms of Bragg reflections obtained from XRD. XRD spectrum showed four characteristic diffraction peaks at 37.9°, 44.1°, 64.5°, and 77.5° which were liable for purity of synthesized nanoparticles. The size calculated using the Scherrer equation was smaller than the sizes obtained from HR-TEM images and hydrodynamic measurements. The hydrodynamic size was the largest, probably because phytochemicals in the extract bonded to the JIF-AuNPs' surface (Ahn et al., 2019).

4.2. Antibacterial studies

Antibacterial activity of JIF-AgNPs has been carried out against gram-positive and gram-negative bacteria. Our findings show that our nanoparticles had an effective antibacterial activity against gram-negative bacteria. This could be owing to the fact that gram-positive organisms have a rigid cell wall, making nanoparticles difficult to enter while the cell walls of gram-negative bacteria are more easily destroyed (Renuka et al., 2020; Sathiyaraj et al., 2020). The mechanism by which a nanoparticle engages with a bacterial membrane is not well established, but studies have found that when nanoparticles are reacted with bacteria, the membrane

morphology changes significantly, resulting in an increase in permeability and regular transport of the plasma membrane, leaving the bacterial cell incapable of proper regulation, resulting in cell death (Ezhilarasi et al., 2020). Cell wall damage (Panda et al., 2016), mitochondrial damage, and DNA damage by nanoparticles have all been proposed as antibacterial mechanisms (Perveen et al., 2018). There have been previous reports of nanoparticles causing similar harm to bacterial cells (Bhushan et al., 2015; Veena et al., 2019). The antibacterial effectiveness of the nanoparticles is mostly determined by particle size, high surface area to volume ratio, and sample morphology. Nanoparticles are often quite small in comparison to bacterial species, allowing them to easily enter the cell (Amanulla et al., 2019; Mobeen et al., 2019). Furthermore, the antibacterial activity of the JIF-AgNPs is dependent on the dose. The findings of this report are consistent with the prior reports (Inbaraj et al., 2020; Muniyappan et al., 2021). The findings revealed that the JIF-AuNPs exhibit potent antibacterial properties.

Nanoparticles have a less substantial influence on the growth of gram-positive bacteria than gram-negative bacteria, according to the MIC against test strains. The fact that a greater zone of inhibition corresponds to a smaller MIC is reflected in the MIC results (Rautela et al., 2019).

5. Conclusion

In conclusion, for the synthesis of nanoparticles, *Jatropha integrifolia* Jacq. flower extract was utilized as a reducing and stabilizing agent. The nanoparticles were spherical and in the 28–43 nm range, according to TEM examination. The crystalline characteristic of AuNPs was studied by SAED and XRD patterns. The antibacterial activity of synthesized nanoparticles was examined using the agar well diffusion method. The MIC was evaluated by broth dilution method, which was found to be 5, 10, 2.5, and 2.5 $\mu\text{g/mL}$ for *B. subtilis*, *S. aureus*, *E. coli*, and *K. pneumoniae*, respectively. The efficacy of these nanoparticles against drug-resistant pathogens makes them a promising therapeutic candidate. As a result, biologically produced nanoparticles have the potential to become future anti-infectives and can be formulated into medicines or topical agents.

Declaration of Competing Interest

The authors declare that they have no known competing financial interests or personal relationships that could have appeared to influence the work reported in this paper.

Acknowledgements

The authors acknowledge the Department of Biotechnology, Thiruvalluvar University for providing facilities to carry out the research work. Also the authors extend their appreciation to the researchers supporting project number (RSP-2021/185), King Saud University, Riyadh, Saudi Arabia.

References

- Adil, M., Khan, T., Aasim, M., Khan, A.A., Ashraf, M., 2019. Evaluation of the antibacterial potential of silver nanoparticles synthesized through the interaction of antibiotic and aqueous callus extract of *Fagonia indica*. *AMB Express* 9. <https://doi.org/10.1186/s13568-019-0797-2>.
- Ahn, E.Y., Jin, H., Park, Y., 2019. Assessing the antioxidant, cytotoxic, apoptotic and wound healing properties of silver nanoparticles green-synthesized by plant extracts. *Mater. Sci. Eng., C* 101, 204–216. <https://doi.org/10.1016/j.msec.2019.03.095>.
- Amanulla, A.M., Sundaram, R., Kaviyarasu, K., 2019. An investigation of structural, magnetical, optical, antibacterial and humidity sensing of Zr(MoO₄)₂-ZrO₂ nanocomposites. *Surf. Interfaces* 16, 132–140. <https://doi.org/10.1016/j.surfin.2019.06.001>.
- Balasubramanian, S., Kala, S.M.J., Pushparaj, T.L., 2020. Biogenic synthesis of gold nanoparticles using *Jasminum auriculatum* leaf extract and their catalytic, antimicrobial and anticancer activities. *J. Drug Delivery Sci. Technol.* 57. <https://doi.org/10.1016/j.jddst.2020.101620>.
- Bhushan, M., Muthukamalam, S., Sudharani, S., Viswanath, A.K., 2015. Synthesis of α -Fe₂-xAgxO₃ nanocrystals and study of their optical, magnetic and antibacterial properties. *RSC Adv.* 5, 32006–32014. <https://doi.org/10.1039/c4ra17259k>.
- Bindhu, M.R., Umadevi, M., 2014. Antibacterial activities of green synthesized gold nanoparticles. *Mater. Lett.* 120, 122–125. <https://doi.org/10.1016/j.matlet.2014.01.108>.
- Devanesan, S., Jayamala, M., AlSalhi, M.S., Umamaheshwari, S., Ranjitsingh, A.J.A., 2021. Antimicrobial and anticancer properties of *Carica papaya* leaves derived di-methyl flubendazole mediated silver nanoparticles. *J Infect Public Health* 14, 577–587. <https://doi.org/10.1016/j.jiph.2021.02.004>.
- Dhanasekar, N.N., Rahul, G.R., Narayanan, K.B., Raman, G., Sakthivel, N., 2015. Green chemistry approach for the synthesis of gold nanoparticles using the fungus *Alternaria* sp. *J. Microbiol. Biotechnol.* 25, 1129–1135. <https://doi.org/10.4014/jmb.1410.10036>.
- Ezhilarasi, A.A., Vijaya, J.J., Kaviyarasu, K., Zhang, X.u., Kennedy, L.J., 2020. Green synthesis of nickel oxide nanoparticles using *Solanum trilobatum* extract for cytotoxicity, antibacterial and photocatalytic studies. *Surf. Interfaces* 20. <https://doi.org/10.1016/j.surfin.2020.100553>.
- Folorunso, A., Akintelu, S., Oyebamiji, A.K., Ajayi, S., Abiola, B., Abdusalam, I., Morakinyo, A., 2019. Biosynthesis, characterization and antimicrobial activity of gold nanoparticles from leaf extracts of *Annona muricata*. *J. Nanostruct. Chem.* 9, 111–117. <https://doi.org/10.1007/s40097-019-0301-1>.
- Gandhi, A.D., Kaviyarasu, K., Supraja, N., Velmurugan, R., Suriyakala, G., Babujanarthanam, R., Zang, Y., Soontarapa, K., Almaary, K.S., Elshikh, M.S., Chen, T.-W., 2021. Annealing dependent synthesis of cyto-compatible nano-silver/calcium hydroxyapatite composite for antimicrobial activities. *Arabian J. Chem.* 14. <https://doi.org/10.1016/j.arabjc.2021.103404>.
- George, A., Raj, D.M.A., Raj, A.D., Irudayaraj, A.A., Arumugam, J., Senthil kumar, M., Prabu, H.J., Sundaram, S.J., Al-Dhahi, N.A., Arasu, M.V., Maaza, M., Kaviyarasu, K., 2020. Temperature effect on CuO nanoparticles: antimicrobial activity towards bacterial strains. *Surf. Interfaces* 21. <https://doi.org/10.1016/j.surfin.2020.100761>.
- Heera, P., Shanmugam, S., 2015. Review article nanoparticle characterization and application: an overview. *Int. J. Curr. Microbiol. App Sci.*
- Hemlata, Meena, P.R., Singh, A.P., Tejavath, K.K., 2020. Biosynthesis of silver nanoparticles using *cuscuta* prothetarium aqueous leaf extract and their antibacterial and antiproliferative activity against cancer cell lines. *ACS Omega* 5, 5520–5528. <https://doi.org/10.1021/acsomega.0c00155>.
- Ibarra-Sánchez, J.J., Fuentes-Ramírez, R., Reyes-Aguilera, J.A., Figueroa-Gerstenmaier, S., Orrantia-Borunda, E., Concha-Guerrero, S.I., de La Rosa, G., 2015. Kinetics for an optimized biosynthesis of silver nanoparticles using Alfalfa extracts. *Int. J. Chem. Reactor Eng.* 13, 359–367. <https://doi.org/10.1515/ijcre-2014-0149>.
- Inbaraj, B.S., Chen, B.Y., Liao, C.W., Chen, B.H., 2020. Green synthesis, characterization and evaluation of catalytic and antibacterial activities of chitosan, glycol chitosan and poly(γ -glutamic acid) capped gold nanoparticles. *Int. J. Biol. Macromol.* 161, 1484–1495. <https://doi.org/10.1016/j.ijbiomac.2020.07.244>.
- Koperuncholan, M., 2015. Bioreduction of chloroauric acid (HAuCl₄) for the synthesis of gold nanoparticles (GNPs): a special empathies of pharmacological activity. *Int. J. Phytopharmacy Res.* 5, 72–80. <https://doi.org/10.7439/ijpp>.
- Krithiga, N., Rajalakshmi, A., Jayachitra, A., 2015. Green synthesis of silver nanoparticles using leaf extracts of *Clitoria ternatea* and *Solanum nigrum* and study of its antibacterial effect against common nosocomial pathogens. <https://doi.org/10.1155/2015/928204>.
- Maiti, S., Krishnan, D., Barman, G., Ghosh, S.K., Laha, J.K., 2014. Antimicrobial activities of silver nanoparticles synthesized from *Lycopersicon esculentum* extract. *J. Anal. Sci. Technol.* 5. <https://doi.org/10.1186/s40543-014-0040-3>.
- Mani, M., Hari Krishnan, R., Purushothaman, P., Pavithra, S., Rajkumar, P., Kumaresan, S., Al Farraj, D.A., Elshikh, M.S., Balasubramanian, B., Kaviyarasu, K., 2021a. Systematic green synthesis of silver oxide nanoparticles for antimicrobial activity. *Environ. Res.* 202. <https://doi.org/10.1016/j.envres.2021.111627>.
- Mani, M., Okla, M.K., Selvaraj, S., Ram Kumar, A., Kumaresan, S., Muthukumar, A., Kaviyarasu, K., El-Tayeb, M.A., Elbadawi, Y.B., Almaary, K.S., Ahmed Almunqedhi, B.M., Elshikh, M.S., 2021b. A novel biogenic *Allium cepa* leaf mediated silver nanoparticles for antimicrobial, antioxidant, and anticancer effects on MCF-7 cell line. *Environ. Res.* 198. <https://doi.org/10.1016/j.envres.2021.111199>.
- Mani, M., Pavithra, S., Mohanraj, K., Kumaresan, S., Alotaibi, S.S., Eraqi, M.M., Gandhi, A.D., Babujanarthanam, R., Maaza, M., Kaviyarasu, K., 2021c. Studies on the spectrometric analysis of metallic silver nanoparticles (Ag NPs) using *Basella alba* leaf for the antibacterial activities. *Environ. Res.* 199. <https://doi.org/10.1016/j.envres.2021.111274>.
- Mariadoss, A.V.A., Ramachandran, V., Shalini, V., Agilan, B., Franklin, J.H., Sanjay, K., Alaa, Y.G., Tawfiq, M.-A., Ernest, D., 2019. Green synthesis, characterization and antibacterial activity of silver nanoparticles by *Malus domestica* and its cytotoxic effect on (MCF-7) cell line. *Microb. Pathog.* 135, 103609. <https://doi.org/10.1016/j.micpath.2019.103609>.
- Mittal, A.K., Kaler, A., Mulay, A.V., Banerjee, U.C., 2013. Synthesis of gold nanoparticles using whole cells of *Guetrichum candidum*. *J Nanopart* 2013. <https://doi.org/10.1155/2013/150414>.
- Mobeen, A., Maria Magdalane, C., Jasmine Shahina, S.K., Lakshmi, D., Sundaram, R., Ramalingam, G., Raja, A., Madhavan, J., Letsholathebe, D., Bashir, A.K.H., Maaza, M., Kaviyarasu, K., 2019. Investigation on antibacterial and photocatalytic degradation of Rhodamine-B dye under visible light irradiation by titanium molybdate nanoparticles prepared via microwave method. *Surf. Interfaces* 17. <https://doi.org/10.1016/j.surfin.2019.100381>.
- Muniyappan, N., Pandeewaran, M., Amalraj, A., 2021. Green synthesis of gold nanoparticles using *Curcuma pseudomontana* isolated curcumin: its characterization, antimicrobial, antioxidant and anti-inflammatory activities. *Environ Chem Ecotoxicol* 3, 117–124. <https://doi.org/10.1016/j.eneco.2021.01.002>.
- Nadaroglu, H., Ince, S., Gungor, A.A., 2017. Green synthesis of gold nanoparticles using quail egg yolk and investigation of potential application areas. *Green Process. Synth.* 6, 43–48. <https://doi.org/10.1515/gps-2016-0091>.
- Nithiyavathi, R., John Sundaram, S., Theophil Anand, G., Raj Kumar, D., Dhayal Raj, A., Al Farraj, D.A., Aljowaie, R.M., AbdelGawwad, M.R., Samson, Y., Kaviyarasu, K., 2021. Gum mediated synthesis and characterization of CuO nanoparticles towards infectious disease-causing antimicrobial resistance microbial pathogens. *J. Infect. Public Health.* <https://doi.org/10.1016/j.jiph.2021.10.022>.
- Otunola, G.A., Afolayan, A.J., Ajayi, E.O., Odeyemi, S.W., 2017. Characterization, antibacterial and antioxidant properties of silver nanoparticles synthesized from aqueous extracts of *Allium sativum*, *Zingiber officinale*, and *Capsicum frutescens*. *Pharmacognosy Magazine* 13, S201–S208. https://doi.org/10.4103/pm.pm_430_16.
- Panda, S., Mohanta, Y., Padhi, L., Park, Y.-H., Mohanta, T., Bae, H., 2016. Large scale screening of ethnomedicinal plants for identification of potential antibacterial compounds. *Molecules* 21. <https://doi.org/10.3390/molecules21030293>.
- Parvekar, P., Palaskar, J., Metgud, S., Maria, R., Dutta, S., 2020. The minimum inhibitory concentration (MIC) and minimum bactericidal concentration (MBC) of silver nanoparticles against *Staphylococcus aureus*. *Biomater. Invest. Dentistry* 7, 105–109. <https://doi.org/10.1080/26415275.2020.1796674>.
- Perveen, S., Safdar, N., Chaudhry, G.E.S., Yasmin, A., 2018. Antibacterial evaluation of silver nanoparticles synthesized from lychee peel: individual versus antibiotic conjugated effects. *World J. Microbiol. Biotechnol.* 34. <https://doi.org/10.1007/s11274-018-2500-1>.
- Priya Velammal, S., Devi, T.A., Amaladhas, T.P., 2016. Antioxidant, antimicrobial and cytotoxic activities of silver and gold nanoparticles synthesized using *Plumbago zeylanica* bark. *J. Nanostruct. Chem.* 6, 247–260. <https://doi.org/10.1007/s40097-016-0198-x>.
- Raja, A., Selvakumar, K., Rajasekaran, P., Arunpandian, M., Ashokkumar, S., Kaviyarasu, K., Asath Bahadur, S., Swaminathan, M., 2019. Visible active reduced graphene oxide loaded titania for photodecomposition of ciprofloxacin and its antibacterial activity. *Colloids Surf., A* 564, 23–30. <https://doi.org/10.1016/j.colsurfa.2018.12.024>.
- Ramesh, R., Catherine, G., John Sundaram, S., Liakath Ali Khan, F., Kaviyarasu, K., 2019. Synthesis of Mn₃O₄ nano complex using aqueous extract of *Helianthus annuus* seed cake and its effect on biological growth of *Vigna radiata*. *Mater. Today: Proc. Elsevier Ltd.* 184–191. <https://doi.org/10.1016/j.matpr.2020.02.883>.
- Rathnakumar, S.S., Noluthando, K., Kulandaiswamy, A.J., Rayappan, J.B.B., Kasinathan, K., Kennedy, J., Maaza, M., 2019. Stalling behaviour of chloride ions: a non-enzymatic electrochemical detection of A-Endosulfan using CuO interface. *Sens. Actuators, B* 293, 100–106. <https://doi.org/10.1016/j.snb.2019.04.141>.
- Rautela, A., Rani, J., Debnath (Das), M., 2019. Green synthesis of silver nanoparticles from *Tectona grandis* seeds extract: characterization and mechanism of antimicrobial action on different microorganisms. *J. Anal. Sci. Technol.* 10. <https://doi.org/10.1186/s40543-018-0163-z>.
- Renuka, R., Devi, K.R., Sivakami, M., Thilagavathi, T., Uthrakumar, R., Kaviyarasu, K., 2020. Biosynthesis of silver nanoparticles using *phyllanthus emblica* fruit extract for antimicrobial application. *Biocatal. Agri. Biotechnol.* 24. <https://doi.org/10.1016/j.bcab.2020.101567>.
- Saqr, A.A., Khafagy, E.S., Alalawi, A., Aldawsari, M.F., Alshahrani, S.M., Anwer, M.K., Khan, S., Lila, A.S., Arab, H.H., Hegazy, W.A.H., 2021. Synthesis of gold nanoparticles by using green machinery: characterization and in vitro toxicity. *Nanomaterials* 11, 1–14. <https://doi.org/10.3390/nano11030808>.
- Sathiyaraj, S., Suriyakala, G., Dhanesh Gandhi, A., Babujanarthanam, R., Almaary, K. S., Chen, T.-W., Kaviyarasu, K., 2021. Biosynthesis, characterization, and antibacterial activity of gold nanoparticles. *J. Infect. Public Health* 14. <https://doi.org/10.1016/j.jiph.2021.10.007>.

- Sathiyaraj, S., Suriyakala, G., Gandhi, A.D., Saranya, S., Santhoshkumar, M., Kavitha, P., Babujanarthanam, R., 2020. Green biosynthesis of silver nanoparticles using vallarai chooranam and their potential biomedical applications. *J. Inorg. Organomet. Polym. Mater.* 30, 4709–4719. <https://doi.org/10.1007/s10904-020-01683-7>.
- Sk, I., Khan, M.A., Haque, A., Ghosh, S., Roy, D., Homechudhuri, S., Alam, M.A., 2020. Synthesis of gold and silver nanoparticles using *Malva verticillata* leaves extract: Study of gold nanoparticles catalysed reduction of nitro-Schiff bases and antibacterial activities of silver nanoparticles. *Curr. Res. Green Sustain. Chem.* 3. <https://doi.org/10.1016/j.crgsc.2020.05.003>.
- Suriyakala, G., Sathiyaraj, S., Gandhi, A.D., Vadakkan, K., Mahadeva Rao, U.S., Babujanarthanam, R., 2021. *Plumeria pudica* Jacq. flower extract - mediated silver nanoparticles: characterization and evaluation of biomedical applications. *Inorg. Chem. Commun.* 126, 108470. <https://doi.org/10.1016/j.inoche.2021.108470>.
- Susan, K.T., JESTEENA, J., Ragunathan, R., 2017. Eco-friendly synthesis of silver nanoparticle using banana (*Musa acuminata* Colla) peel, its phytochemical, antimicrobial and anticancer activity. *Int. J. Recent Sci. Res.* 8, 21098–21106. <https://doi.org/10.24327/ijrsr.2017.0810.1014>.
- Theophil Anand, G., Renuka, D., Ramesh, R., Anandaraj, L., John Sundaram, S., Ramalingam, G., Magdalane, C.M., Bashir, A.K.H., Maaza, M., Kaviyarasu, K., 2019. Green synthesis of ZnO nanoparticle using *Prunus dulcis* (Almond Gum) for antimicrobial and supercapacitor applications. *Surf. Interfaces* 17, 100376. <https://doi.org/10.1016/j.surfin.2019.100376>.
- Veena, S., Devasena, T., Sathak, S.S.M., YASASVE, M., Vishal, L.A., 2019. Green synthesis of gold nanoparticles from *Vitex negundo* leaf extract: characterization and in vitro evaluation of antioxidant-antibacterial activity. *J. Cluster Sci.* 30, 1591–1597. <https://doi.org/10.1007/s10876-019-01601-z>.